

Article

Balanced Anti-Corrosion Action of Reduced Graphene Oxide in Zn-Al Coating during Medium-Term Exposure to NaCl Solution

Qifeng Shi ^{1,2,3}, Huishu Wu ^{1,3,4,*}, Peipei Zhang ^{1,3}, Dongsheng Wang ^{1,2,3,5,*} , Jingwen Wang ^{1,2,3,5} and Xiaohua Jie ⁴

¹ College of Mechanical Engineering, Tongling University, No. 4 Cuihu Road, Tongling 244000, China; 13431093689@163.com (Q.S.); wangjingwen@tlu.edu.cn (J.W.)

² Advanced Copper-Based Materials Industry Generic Technology Research Center of Anhui Province, Tongling 244000, China

³ Key Laboratory of Additive Manufacturing, Anhui Higher Education Institutes, Tongling University, No. 4 Cuihu Road, Tongling 244000, China

⁴ School of Materials and Energy, Guangdong University of Technology, Guangzhou 510006, China; cnxyyz3@gdut.edu.cn

⁵ Key Laboratory of Construction Hydraulic Robots, Anhui Higher Education Institutes, Tongling 244000, China

* Correspondence: ggwuhuishu@163.com (H.W.); wangdongsheng@tlu.edu.cn (D.W.)

Abstract: Considering the electronegativity and shielding anti-sepsis characteristic of reduced graphene oxide (G), we design a Zn-Al coating with embedded G (Zn-G/Al) on low-carbon steel using the low-pressure cold spray (LPCS) method. In this method, G-coated Al powders (G/Al) prepared using in situ reduction and Zn powders were mixed as a raw material for spraying. Embedding G could boost the cathodic protection performance of Zn-Al (70 wt.% zinc and 30 wt.% aluminum) coating, as has been confirmed in previous work. In this work, the microstructure, composition and electrochemical parameters of Zn-G/Al coating during full immersion were measured to investigate G's effect on the corrosion protection properties of the Zn-Al coating. The test results showed that embedded G could facilitate the generation of many corrosion products and pile on the coating surface to form a corrosion product film during full immersion. The corrosion product film on the Zn-0.2 wt.%G/Al coating surface demonstrated an excellent protective property, which reflects the fact that the E_{corr} and i_{corr} values for Zn-0.2 wt.%G/Al after 20d immersion ($E_{corr} = -1.143 V_{vs.SCE}$, $i_{corr} = 49.96 \mu A/cm^2$) were lower than the initial value ($E_{corr} = -1.299 V_{vs.SCE}$, $i_{corr} = 82.16 \mu A/cm^2$). It can be concluded that adding an appropriate amount of G to the coating can balance the cathodic protection and shielding property of the coating. The equilibrium mechanism was also analyzed in this work.

Keywords: Zn-Al coating; reduced graphene oxide; shielding protection; electrical conductivity; low-pressure cold sprayed; low-carbon steel



Citation: Shi, Q.; Wu, H.; Zhang, P.; Wang, D.; Wang, J.; Jie, X. Balanced Anti-Corrosion Action of Reduced Graphene Oxide in Zn-Al Coating during Medium-Term Exposure to NaCl Solution. *Coatings* **2023**, *13*, 1570. <https://doi.org/10.3390/coatings13091570>

Academic Editor: Alina Vladescu

Received: 7 August 2023

Revised: 4 September 2023

Accepted: 5 September 2023

Published: 8 September 2023



Copyright: © 2023 by the authors. Licensee MDPI, Basel, Switzerland. This article is an open access article distributed under the terms and conditions of the Creative Commons Attribution (CC BY) license (<https://creativecommons.org/licenses/by/4.0/>).

1. Introduction

Coating technology is an economical and effective surface treatment technology, which is widely used to prevent the corrosion and destruction of metal constructions in a marine environment [1,2]. A cathodic protection coating is one of many protective coatings [3,4]. The protection mechanism of cathodic protection coating is reflected in multiple ways. On the one hand, cathodic protection coatings act as a sacrificial anode to guard the substrate by making use of the potential difference between it and the substrate. On the other hand, the coating is also an excellent physical shielding coating, involving the shielding of the coating itself and the blocking of the corrosion products forming a film via the degradation of the coating [5].

Zn-based coatings are a promising cathodic protective coating that can prevent the corrosion of carbon steel due to their lower self-corrosion potential (around $-1.1 V_{SCE} \sim -1.3 V_{SCE}$)

compared to that of low-carbon steel ($-0.72 V_{SCE}$) [6–11]. For instance, the self-corrosion potential for a hot-dipped Zn-Al coating is $-1.05 V_{SCE}$ [6] and that for cold-sprayed Zn-xNi is around $-0.98 V_{SCE} \sim -1.01 V_{SCE}$ [7]. Among the Zn-based composite coatings, the Zn-Al coating has certain advantages. For example, the potential difference between Zn and Al is tiny, meaning that the galvanic corrosion tendency in the coating is not obvious. Moreover, the corrosion products of Zn-Al are mainly insoluble layered double hydroxides (LDHs), which could delay the penetration of the corrosive medium [10]. Therefore, Zn-Al coatings often act as an anode to protect low-carbon steel.

Many researchers have focused on the fabrication and anti-corrosion performance of Zn and Zn-Al coatings as a protective coating for steel in marine environments [9–14]. Tachiban et al. [9] studied the corrosion resistance of hot-dipped Zn and Zn-Al coatings in a coastal area. Xue et al. [11] investigated the microstructure and corrosion resistance behavior of a Zn-Al coating co-deposited on low-carbon steel via pack cementation. How the Al content affects the corrosion behavior of arc-sprayed Zn-Al coatings was further studied in the work of Zhu et al. [12]. The results indicated that the Zn-Al coating has a higher corrosion resistance to seawater than the pure Zn coating, and Zn-30Al exhibited the highest corrosion resistance. The experiments of Kim et al. [13] made clear that Zn-Al coatings improve the corrosion resistance of the base material in marine environments by forming ZnO and $Zn_5(OH)_8Cl_2 \cdot H_2O$ corrosion products. However, the pure Zn-30Al coating represented a limited cathodic protection efficiency in a harsh corrosive environment [15].

Usually, the potential difference between the coating and the substrate is increased to improve the efficiency of the cathodic protection of the coating. Liu [16] and Zhu et al. [17] added active elements Mg and Cu to a Zn-Al coating, respectively. Their experiments show that the obtained coatings have a lower electrode potential and express an enhanced cathodic protection efficiency. As a rule, a lower electrode potential means a higher active dissolution rate, which greatly reduces the service life of the coating. Hence, the key point when improving the comprehensive protective performance of Zn-Al coatings is to attain a balance between sacrificial behavior and dissolution resistance. Huang [15] increased the cathodic protection without causing too fast a coating dissolution by matching the ratio of Zn and Al in a Zn-Al coating. Arrighi [4] added Ce(III) as a potential corrosion inhibitor of sacrificial Zn-Fe coatings that were electrodeposited on steel. Liu [16] added an active Mg element to Al-Zn-Si, which decreased the electrode potential and enhanced the cathodic protection efficiency of an Al-Zn-Si alloy. Moreover, an appropriate amount of magnesium in the alloy can promote the formation of a MgZn phase, which could inhibit the corrosion of the alloy. This means that the appropriate alloying element Mg has a balancing effect on the service life and cathodic protection property of Al-Zn-Si-Mg alloys. Is there an adequate additive that could enhance both the service life and cathodic protection property of Zn-Al coatings?

Reduced graphene oxide (rGO; in this work, rGO is denoted as G) is a form of graphene. It is a special corrosion protection material with a large surface area and strong conductivity and a promising and versatile additive [18]. The anti-sepsis characteristics of graphene are related to its distribution state and the properties of the composite materials. When a complete graphene coating is distributed on the substrate surface [19], or a graphene composite is made with organic and inorganic coatings [20], graphene mainly plays a shielding role, using its large surface area to extend the propagation path of corrosive media. If graphene is composited with metals, the graphene in these composites may promote the dissolution of metal by accelerating electron transfer when in a corrosive environment, by which passive metals could form a passive film [21] and active metal would rapidly be degraded [22,23]. Based on the abovementioned points, it can be speculated that G is a suitable additive, which can enhance both the service life and cathodic protection properties of a Zn-Al coating, and the key is to distribute G evenly in the coating.

We deposited a Zn-G/Al composite coating on low-carbon steel using LPCS [24,25]. Using G-coated Al powders prepared by chemical reduction as a feedstock, G was successfully embedded in the interface of Zn and Al. According to experiments [24], G lowered the

potential of the Zn-G/Al coating and thus enhanced its potential difference with the substrate. In this way, the boosting potential difference facilitates the cathode polarization behavior and induces the formation of corrosion products when in a harsh environment. In this work, Zn-G/Al composite coatings were immersed in NaCl solution, and the medium-term immersion behavior was observed to study how the embedded G affects the medium-term protection performance of Zn-G/Al coatings.

2. Experiments

2.1. Preparation and Characteristics of Zn-*x* wt.%G/Al Coatings

Zn-*x* wt.%G/Al coatings were deposited with 70 wt.% zinc (Zn) powders and 30 wt.% G-coated aluminum (G/Al) powders; *x* represents the mass G-to-Al particle ratio, which was 0, 0.1, 0.2 wt.% and 0.3 wt.%, respectively. G-coated Al powders were prepared by the chemical reduced method, as shown in ref. [24]. Taking the preparation method of 0.1 wt.%G/Al powders as an example: 20 mg graphene oxide (GO) was sonicated in 100 mL deionized (DI) water until it was well-dispersed in solvent. Afterward, 20 g pure Al powder was added to the dispersed GO solution and stirred until the solution became colorless and transparent. Then, the mixture was filtered and cleaned with ethanol, and finally dried under vacuum at 50 °C for 8 h to obtain the 0.1 wt.%G/Al powders. Due to the reduction in Al, GO was reduced to rGO and coated on the surface of the Al powder to form reduced graphene-oxide-coated Al powder (rGO/Al, namely G/Al). The preparation process of 0.2 wt.%G/Al and 0.3 wt.%G/Al powders is the same as for 0.1 wt.%G/Al; the only difference is the dispersed GO solution, which is 40 mg/200 mL for 0.2 wt.%G/Al and 60 mg/300 mL for 0.3 wt.%G/Al.

Zn-*x* wt.%G/Al coatings were deposited on a low-carbon steel plate with the size of 2 mm × 10 mm × 10 mm (low-carbon steel is composed of 0.16% C, 0.53% Mn, 0.30% Si, 0.055% S, 0.045% P and balanced Fe) by low-pressure cold spray from the Obninsk Center for Powder Spraying (Russia). Powders blended with 70 wt.% Zn and 30 wt.% G/Al were used as raw spraying materials via mechanical vibration. Using compressed air as the driving gas for the particles, the temperature and pressure of the air were set as 400 °C and 0.8 MPa, respectively. The surface optical images and cross-section SEM images of the obtained Zn-*x* wt.%G/Al coatings are depicted in our previous work [25].

2.2. Testing Barrier Properties of Zn-*x* wt.%G/Al Coatings

The medium-term shielding performance for the coating was evaluated by a full-immersion test. The full-immersion test was carried out in 3.5 wt.% NaCl solution at 25 °C; immersion time was 20 d. Before testing, the coating surface was sanded with emery papers up to a grit size of 1200# and mechanically polished; after testing, the samples were washed and dried. After that, the coating sample was molded in epoxy resin, with a 1.0 cm² area exposed to the solution. The surface corrosion morphology of the coatings after 10 and 20 days' immersion was first investigated by macro-observations and then analyzed by a field emission scanning electronic microscope (FE-SEM, Hitachi S-4800, Tokyo, Japan). The component characteristics of corrosion products after 10 and 20 days' immersion were detected on an X-ray diffraction diffractometer (XRD, D/Max 2500 PC) with a Cu target ($\lambda = 0.154$ nm) at a scanning rate of 4/min ranging from 10° to 80°.

The electrochemical corrosion behavior of the coating was investigated by testing the potentiodynamic polarization (PDP) and carrying out electrochemical impedance spectroscopy (EIS). An electrochemical test was performed in a conventional three-electrode system at room temperature. The working electrode was the exposed surface of the coating sample. A saturated calomel electrode (SCE) and platinum foil were used as the reference and auxiliary electrode, respectively. The PDP experiments of the samples were conducted at the beginning of immersion (2 h) and after 20 days' immersion. The polarization data were acquired at a sweep rate of 1 mV/s, from 100 mV below the open-circuit potential (OCP) to 300 mV above the OCP. The self-corrosion potential (E_{corr}) and self-corrosion current density (i_{corr}) values of the tested coatings were obtained using Tafel extrapolation.

EIS for the samples was acquired at 1, 5, 10 and 20 days' immersion, respectively. The EIS test was conducted at OCP; a single-amplitude perturbation of 5 mV was applied with a frequency range from 10^5 Hz to 10^{-2} Hz. ZsimpWin was used for the data fitting of impedance spectra. For accuracy, three parallel samples were tested in all electrochemical experimental tests and the average value was reported.

3. Results and Discussion

The SEM morphologies of Zn powders, Al powders and 0.2 wt.%G/Al are presented in Figure 1. The size for Zn and Al is around 15–20 μm ; some wrinkles appeared on the 0.2 wt.%G/Al powders' surface, as shown in Figure 1c. A Raman test was conducted to measure G; D (1310 cm^{-1}) and G (1595 cm^{-1}) peaks were observed on the Raman spectrum acquired from the surface of 0.2 wt.%G/Al powder (Figure 1d). As depicted, the D/G intensity ratio of G (1.13) was higher than that of GO (0.84), which confirmed that GO was reduced and coated on the Al powder surface.

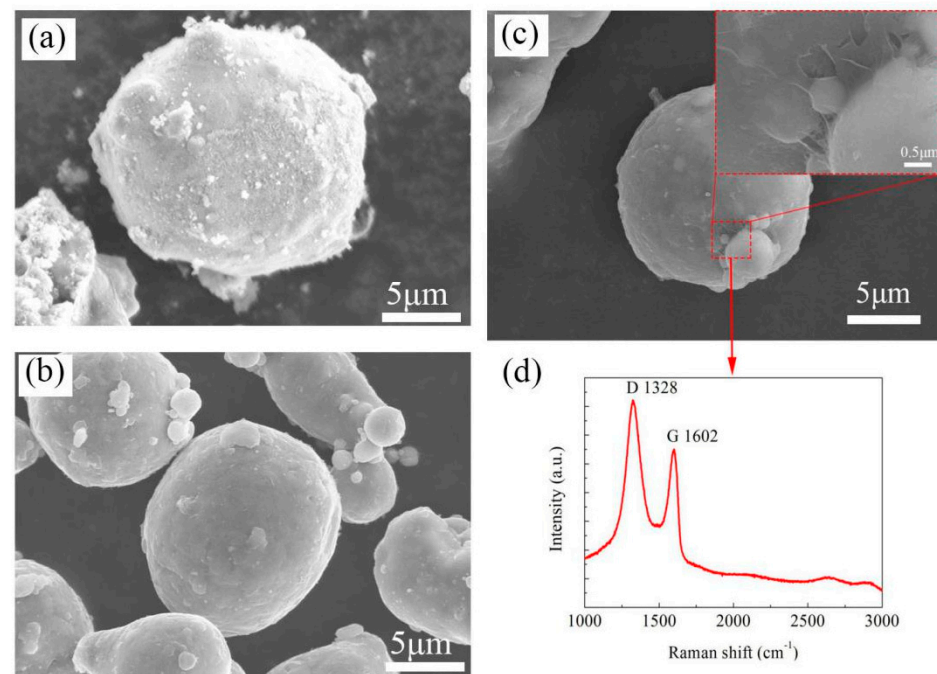


Figure 1. The morphology of Zn powders (a), Al powders (b) and 0.2 wt.%G/Al powders (c), and the Raman spectrum acquired from the surface of 0.2 wt.%G/Al powder (d).

Figure 2 shows the macroscopic corrosion appearance of the Zn-x wt.%G/Al coating after immersion in 3.5 wt.% NaCl solution for 5 d, 10 d and 20 d. As presented, the white corrosion products gradually covered the coating surface during the immersion time. During the early and middle immersion time (5 d and 10 d), the area of the coating surface covered by corrosion products differed. The cover area is arranged in the order of Zn-0.2 wt.%G/Al, Zn-0.1 wt.%G/Al, Zn-0.3 wt.%G/Al, Zn-Al, from large to small. The results indicate that the presence of G in the coating could accelerate the dissolution of the coating when in a corrosive solution, and the Zn-0.2 wt.%G/Al coating experienced the fastest corrosion rate at the initial immersion time. With prolonged immersion, the corrosion products on Zn-x wt.%G/Al coatings become more compact and evenly distributed.

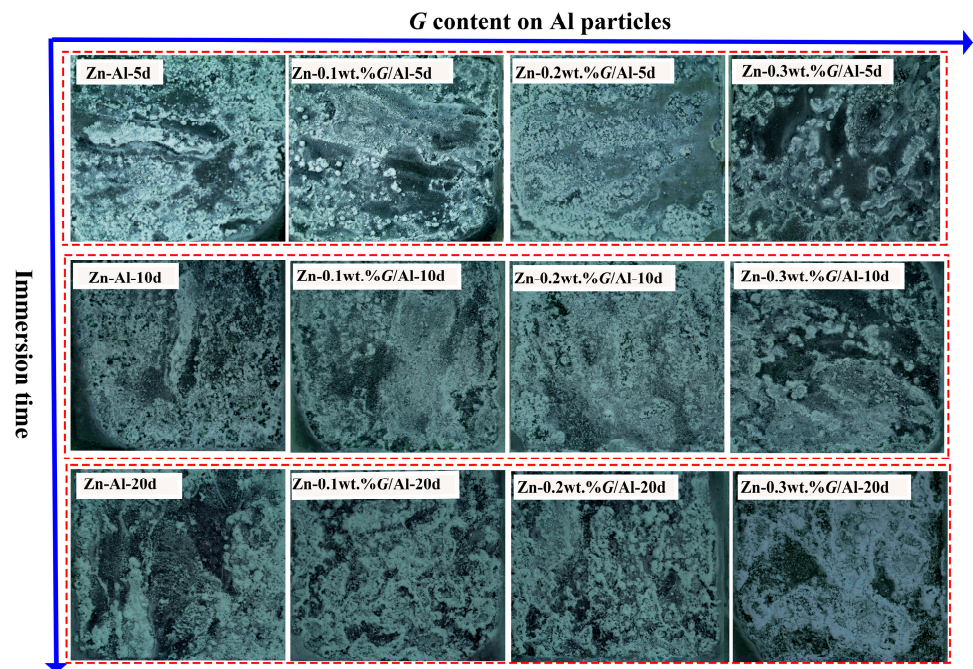


Figure 2. Surface macro-morphology of Zn-x wt.%G/Al coatings after immersion in NaCl solution.

Figure 3 shows the SEM morphology of corrosion products generated on Zn-x wt.%G/Al coatings' surface after immersion in 3.5 wt.% NaCl for 10 d. As demonstrated in Figure 3a, some loose corrosion products accumulated on the Zn-Al coating surface, and part of the bare coating substrate was still exposed after 10 d of immersion. The Zn-0.1 wt.%G/Al and Zn-0.3 wt.%G/Al coatings' surfaces were covered by a mass of nanoplatelets with a size of 2–3 μm and the nanoplatelets were vertically cross-linked, as presented in Figure 3b,d. Corrosion products on the Zn-0.2 wt.%G/Al coating were the most compact, and nanosheets for the products were very tiny, with a size of 2–3 μm , as shown in Figure 3c.

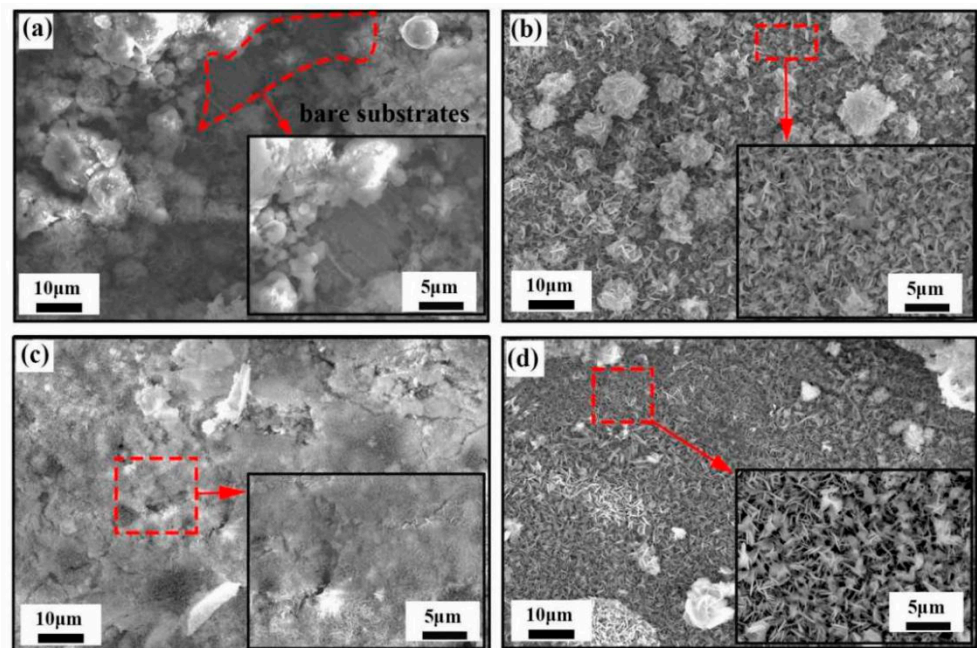


Figure 3. Surface SEM morphology for Zn-x wt.%G/Al coatings after immersion in NaCl solution for 10 d. (a) Zn-Al coating. (b) Zn-0.1 wt.%G/Al. (c) Zn-0.2 wt.%G/Al. (d) Zn-0.3 wt.%G/Al.

Figure 4 shows the SEM morphology of corrosion products generated on Zn-x wt.%G/Al coatings' surface after immersion in 3.5 wt.% NaCl solution for 20 d. After 20 d immersion, clusters of corrosion products accumulated loosely on the Zn-Al coating surface (Figure 4a), with apparent gaps between the cluster layers. Rod-shaped nanoparticles clustered and densely covered the Zn-0.1 wt.%G/Al coating surface to form a film of corrosion products, as shown in Figure 4b. For the Zn-0.2 wt.%G/Al coating after 20 d immersion, as presented in Figure 4c, the corrosion product layer is compact and composed of nanosheets. Flake-like corrosion products were formed on the Zn-0.3 wt.%G/Al coating surface, and some cracks and holes occurred on the corrosion product layer's surface.

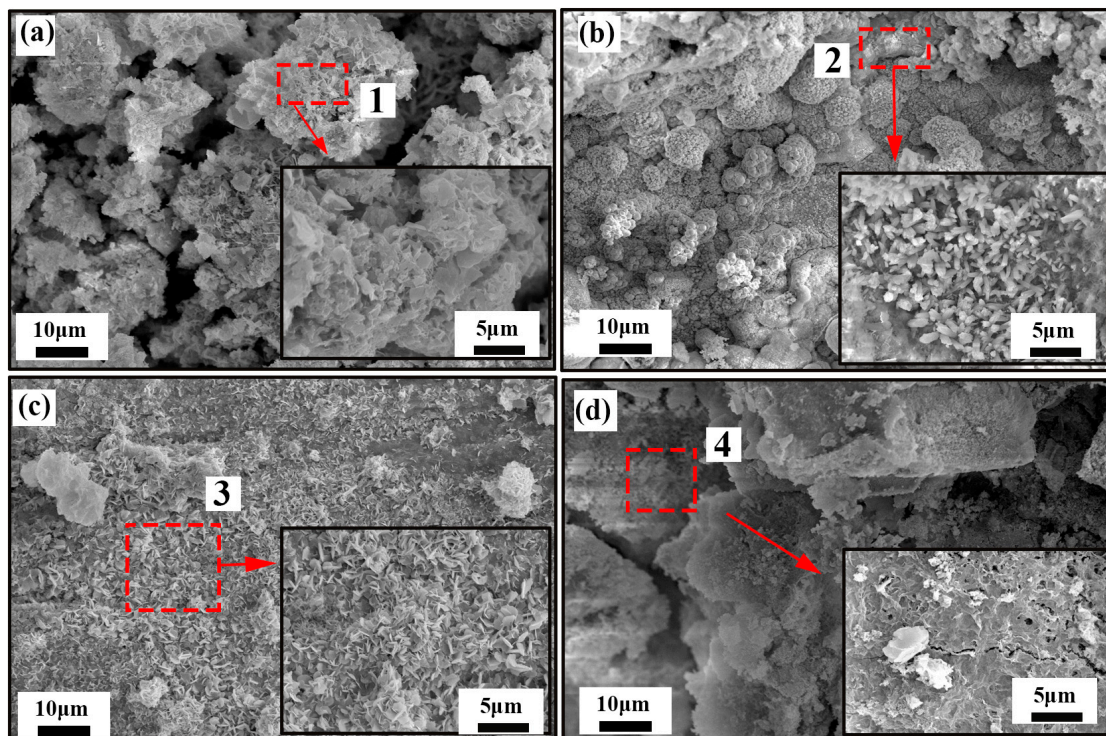


Figure 4. Surface SEM morphology for Zn-x wt.%G/Al coatings after immersion in 3.5 wt.% NaCl solution for 20 d. (a) Zn-Al coating. (b) Zn-0.1 wt.%G/Al. (c) Zn-0.2 wt.%G/Al. (d) Zn-0.3 wt.%G/Al.

Figure 5 is EDX results acquired from regions 1, 2, 3 and 4 shown in Figure 4. After 20 d immersion, the corrosion products are mainly composed of elements Zn, Al, Cl, C and O. The element Cl came from corrosive media, and C is derived from CO_2 that dissolved in solution. As shown in EDX results, it can be seen that O content in corrosion products formed on the Zn-0.2 wt.%G/Al surface is highest, which may be related to the formation of $\text{ZnAl}_2\text{CO}_3(\text{OH})_{16}\cdot 4\text{H}_2\text{O}$.

Figure 6 shows the XRD results for corrosion products on the Zn-x wt.%G/Al coating after 10 d and 20 d immersion in NaCl solution. After 10 d immersion, an outstanding peak clearly appeared, centered around 11.3° , 43° and associated with hydrozincite [22]. Peaks caused by $\text{Zn}_4\text{CO}_3(\text{OH})_6\cdot\text{H}_2\text{O}$ were present at 37° , 54° and 72° in the XRD pattern [20]. The peak of zinc oxide (ZnO) at 39.5° [26] was relatively higher than the peaks of simonkolleite ($\text{Zn}_5(\text{OH})_8\text{Cl}_2$) at 11.3° , $\text{ZnAl}_2\text{CO}_3(\text{OH})_{16}\cdot 4\text{H}_2\text{O}$ around 11.3° and 43° and $\text{Zn}_4\text{CO}_3(\text{OH})_6\cdot\text{H}_2\text{O}$ at 54° and 72° [10]. There were some changes in the intensity of the diffraction peak of the corrosion products when immersion time was prolonged to 20 d, as shown in Figure 6. The diffraction peak intensity of ZnO at 39.5° decreased, and the peak intensity of $\text{Zn}_4\text{CO}_3(\text{OH})_6\cdot\text{H}_2\text{O}$ at 54° , 72° and $\text{ZnAl}_2\text{CO}_3(\text{OH})_{16}\cdot 4\text{H}_2\text{O}$ at 43° was strengthened. Some mini peaks around 33.5° , ascribed to $\text{Zn}_5(\text{OH})_8\text{Cl}_2$ and $\text{Zn}_4\text{CO}_3(\text{OH})_6\cdot\text{H}_2\text{O}$, successively appeared, which may be due to the transformation of ZnO. ZnO is unstable, which means that it readily reacts with water and gradually turns into simonkolleite with

low dissolving properties in water. After immersion in NaCl solution, simonkolleite could provide protection for the coating. For Zn-0.2 wt.%G/Al coating, the diffraction peak intensity of $ZnAl_2CO_3(OH)_{16}\cdot 4H_2O$ at 43° strengthened remarkably, which may be related to the translation of Al.

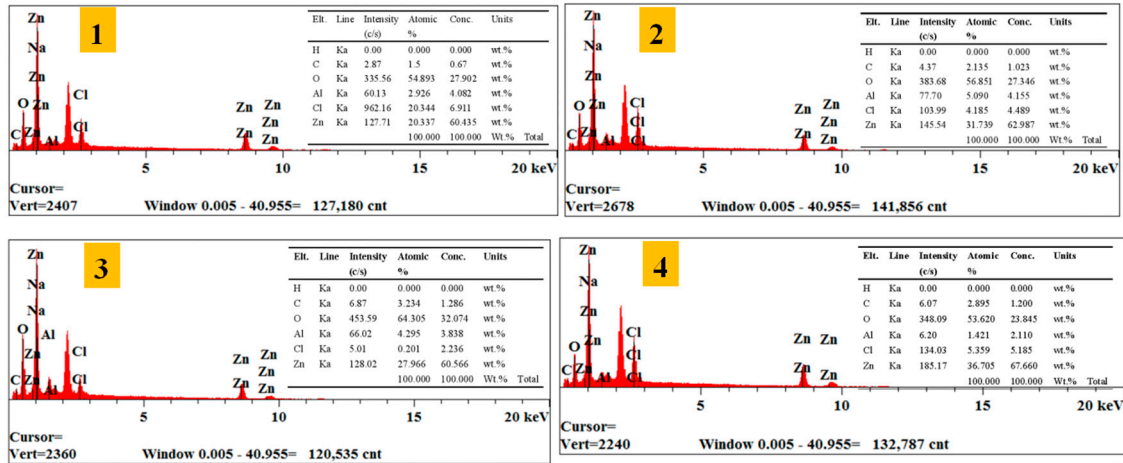


Figure 5. EDX analysis of corrosion products generated on Zn-x wt.%G/Al coatings after immersion for 20 d in NaCl solution, 1, 2, 3, 4 is corresponding with point 1, 2, 3, 4 in Figure 4.

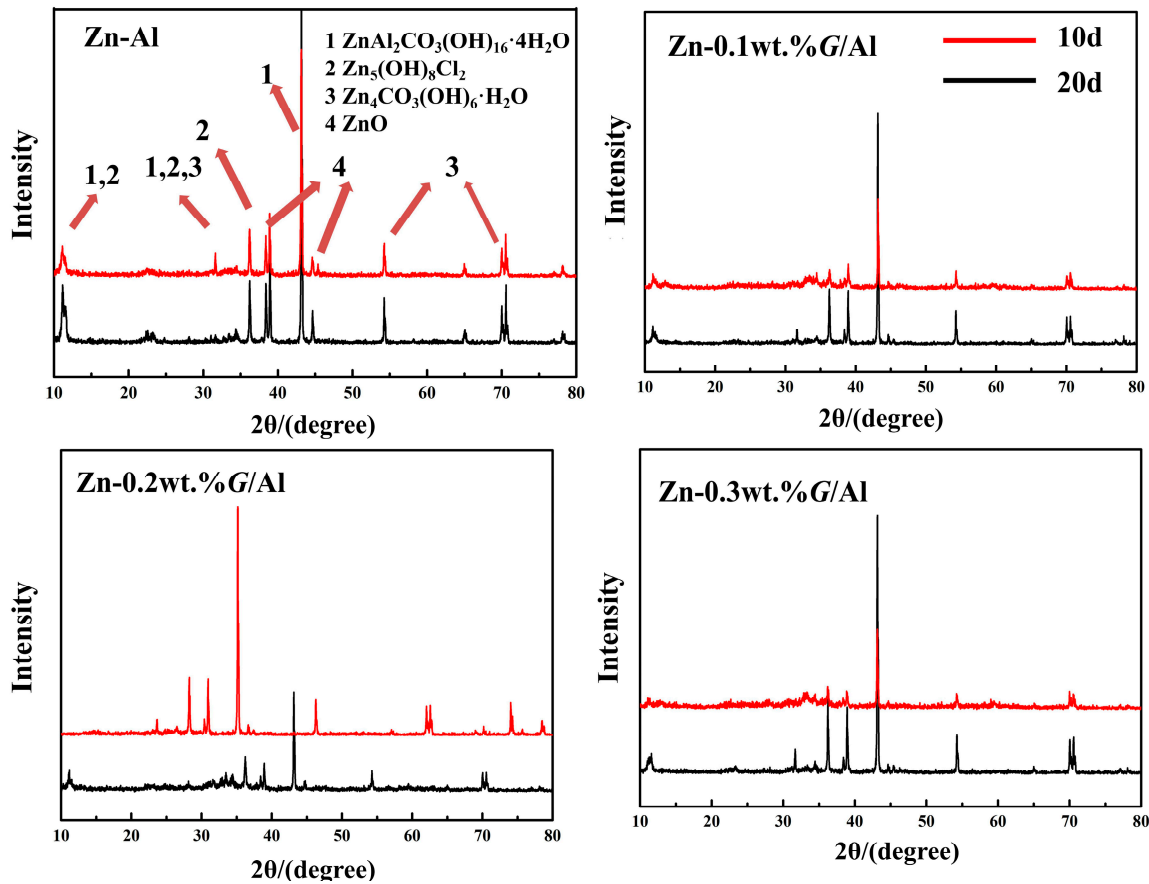


Figure 6. XRD results for corrosion products on Zn-x wt.%G/Al coatings after 10 d and 20 d immersion in 3.5 wt.% NaCl, respectively.

Figure 7 presents the potentiodynamic polarization curves (PPCs) of Zn-x wt.%G/Al coatings after immersion for 2 h and 20 d. The specific E_{corr} and i_{corr} values fitted from the PPC are displayed in Table 1. For the Zn-Al coating, the E_{corr} value of the Zn-Al coating after immersion for 2 h is $-1.055 V_{SCE}$; the value for the coating after 20 d immersion decreased to $-1.083 V_{SCE}$. After 20 d immersion, the i_{corr} value for the Zn-Al coating is $15.8 \mu A/cm^2$, which is two and a half times higher than the value of the Zn-Al coating after immersion for 2 h ($6.508 \mu A/cm^2$). The E_{corr} values for Zn-0.1 wt.%G/Al, Zn-0.2 wt.%G/Al and Zn-0.3 wt.%G/Al coatings are $-1.180 V_{SCE}$, $-1.143 V_{SCE}$ and $-1.152 V_{SCE}$ after 20 d immersion, which are elevated compared with the coating values acquired at 2 h immersion time. The variation trend of the i_{corr} value for the Zn-G/Al coating is the opposite. The i_{corr} value for Zn-0.1 wt.%G/Al and Zn-0.3 wt.%G/Al coatings increased, but that for the Zn-0.2 wt.%G/Al coating decreased.

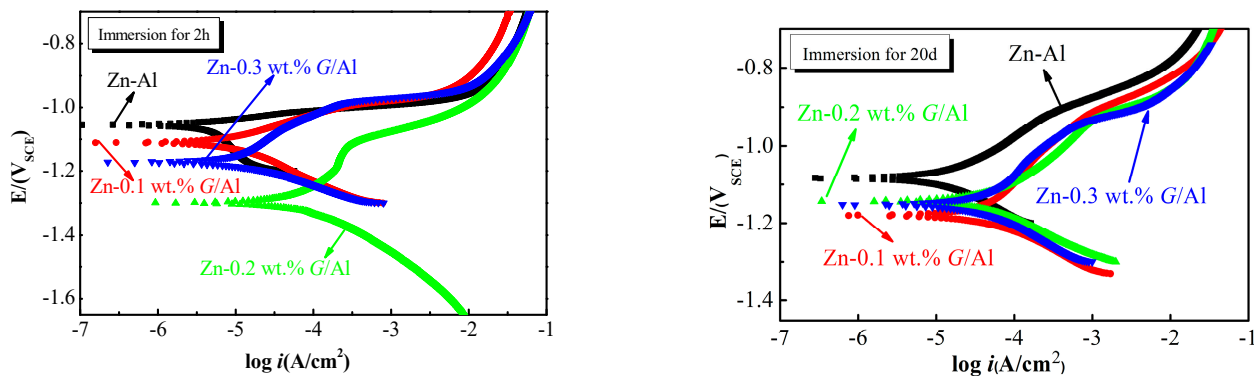


Figure 7. Polarization curves for Zn-x wt.%G/Al coatings after immersion for 2 h and 20 d.

Table 1. E_{corr} and I_{corr} values fitted from PPS for Zn-x G/Al composite coatings after immersion in 3.5 wt. % NaCl solution for 2 h and 20 d.

Coatings	E_{corr} (V _{vs.SCE})		I_{corr} ($\mu A/cm^2$)	
	2 h	20 d	2 h	20 d
Zn-Al	-1.055	-1.083	6.508	15.8
Zn-0.1 wt.%G/Al	-1.187	-1.180	55.59	58.07
Zn-0.2 wt.%G/Al	-1.299	-1.143	82.16	49.96
Zn-0.3 wt.%G/Al	-1.172	-1.152	14.58	52.06

In PPCs, the E_{corr} value indicates the corrosion tendency of the coating and a higher E_{corr} value means a lower corrosion tendency; the i_{corr} value represents the corrosion rate of the coating and the value of i_{corr} is inversely proportional to its anti-corrosion properties. For the steel with a protective coating, the higher the potential difference between the coating and steel matrix, the stronger the coating’s propensity for cathodic protection. A higher corrosion current density indicated a better cathodic protection efficiency. Compared with the E_{corr} value for steel ($-0.72 V_{SCE}$), Zn-G/Al coating values were all below $-1V_{SCE}$, which indicates that all Zn-G/Al coatings are cathodic protection coatings. Increasing with immersion time, the E_{corr} values for Zn-0.1 wt.%G/Al, Zn-0.2 wt.%G/Al and Zn-0.3 wt.%G/Al coatings at 20 d increased by 0.5%, 12% and 1.7%, respectively, in comparison with the value at the initial immersion time but were still lower than that of steel ($-0.72 V_{SCE}$). Therefore, the coating could protect steel through its sacrificial anode action during full immersion.

Cathodic protection is the method of sacrificing the anode to avoid the corrosion of the cathode. The sacrificial ability of the anode increases with the increase in dissolution rate of the coating layer, while the large dissolution rate of the coating layer decreases service life for the coating [8]. The key point is the balance between sacrificial behavior and

dissolution resistance. In the work of Jonathan Elvins et al. [27], the effect of magnesium additions on cut edge corrosion resistance of zinc aluminum alloy galvanized steel was studied. They measured individual anodic activity against anode number for the cut edge by SVET. Results indicated that the addition of Mg resulted in an increase in zinc loss, an increase in active anode numbers and an increase in the number of long-lived anodes. Ding et al. [23] prepared graphene/zinc-containing coatings on steel, and electrochemical test results indicated that 0.3%graphene-70%Zn coating has the highest current corrosion density, which presented that adding graphene prolonged the duration and increased the values of the stable cathodic protection currents of the coating. Hence, a higher cathodic protection efficiency calls for a higher corrosion current density during the process of cathodic protection. As shown in Table 1, the i_{corr} value for the Zn-G/Al coating is higher than that of Zn-Al, which means that adding G to the coating could enhance the activity and strengthen the cathodic protection effect of the Zn-Al composite coating during the full-immersion process.

During the anodic protection of metals, the anodic protection coating is also required to have a low corrosion rate to extend its service life. However, the higher the anodic protection efficiency of the coating, the higher the corrosion rate. Therefore, if the coating can generate a protective corrosion product layer to reduce the degradation rate during the anodic protection process, then this contradiction may be alleviated. It is surprising that the i_{corr} value for Zn-0.2 wt.%G/Al went down after 20 d immersion compared with the value at the initial immersion time, which demonstrated that the corrosion products generated on the Zn-0.2 wt.%G/Al coating could delay the degradation and prolong the service life of the coating. Therefore, we conclude that inserting G into the coating endowed the coating with an enduring activity and equipped it with a persistent cathodic protection ability during full immersion. When the G content in powders of the Al surface is 0.2 wt.%, the obtained composite coating surface generated a protective corrosion product film after 20d immersion, which could retard the degradation of coating.

Compared with casted Zn-Al alloy [28] or hot-dipped Zn-Al composite coating (E_{corr} is around -1.0) [16], Zn-G/Al coating has an excellent cathodic protection efficiency. However, the i_{corr} value for Zn-G/Al coating is still higher than that of traditional cathodic protection coating.

To illustrate the equilibrium effect, the impedance change for Zn-Al and Zn-0.2 wt.%G/Al coatings during the full immersion is presented in Figure 8. Actually, Zn-G/Al coating during immersion experienced two processes: firstly, the generation of corrosion products; secondly, the compaction of corrosion products. The densification of corrosion products is related to activity of the coating. For the Zn-Al coating, the electrochemical impedance spectrum (EIS) after 5–10 d immersion was fitted by the equivalent circuit $R_s(Q_1(R_1Q_2(R_2Z_w)))$ [29]. R_s , corresponding to a high-frequency region, represents the resistance of the electrolyte; Q_1 and R_1 are linked to the capacitance and resistance of the corrosion products stacked on the coating surface, respectively. The reactions of the coating are described by the charge transfer resistance R_2 and the double-layer capacitance Q_2 which correspond to the low-frequency region. As demonstrated in EIS curves, a 45° near-line appears in the low-frequency region, which is caused by the diffusion of the porous corrosion product layer, for which a corresponding semi-infinite-length Warburg element Z_w is added in series with R_2 . The EIS after 20 d immersion was fitted by the equivalent circuit $R_s(Q_1(R_1(R_2Q_2)))$ [30]; there was no apparent diffusion phenomenon due to the corrosion product layer has basically formed. For the Zn-0.2 wt.%G/Al coating, before 5 d immersion, EIS curves were fitted by an equivalent circuit of $R_s(Q_1(R_1Q_2(R_2Z_w)))$. After 10 d immersion, corrosion products were generated and stacked on the Zn-0.2 wt.%G/Al coating surface to form a layer. Therefore, the equivalent circuit $R_s(Q_1(R_1(R_2Q_2)))$ can be used to fit the EIS curve of the coating after 10 d immersion.

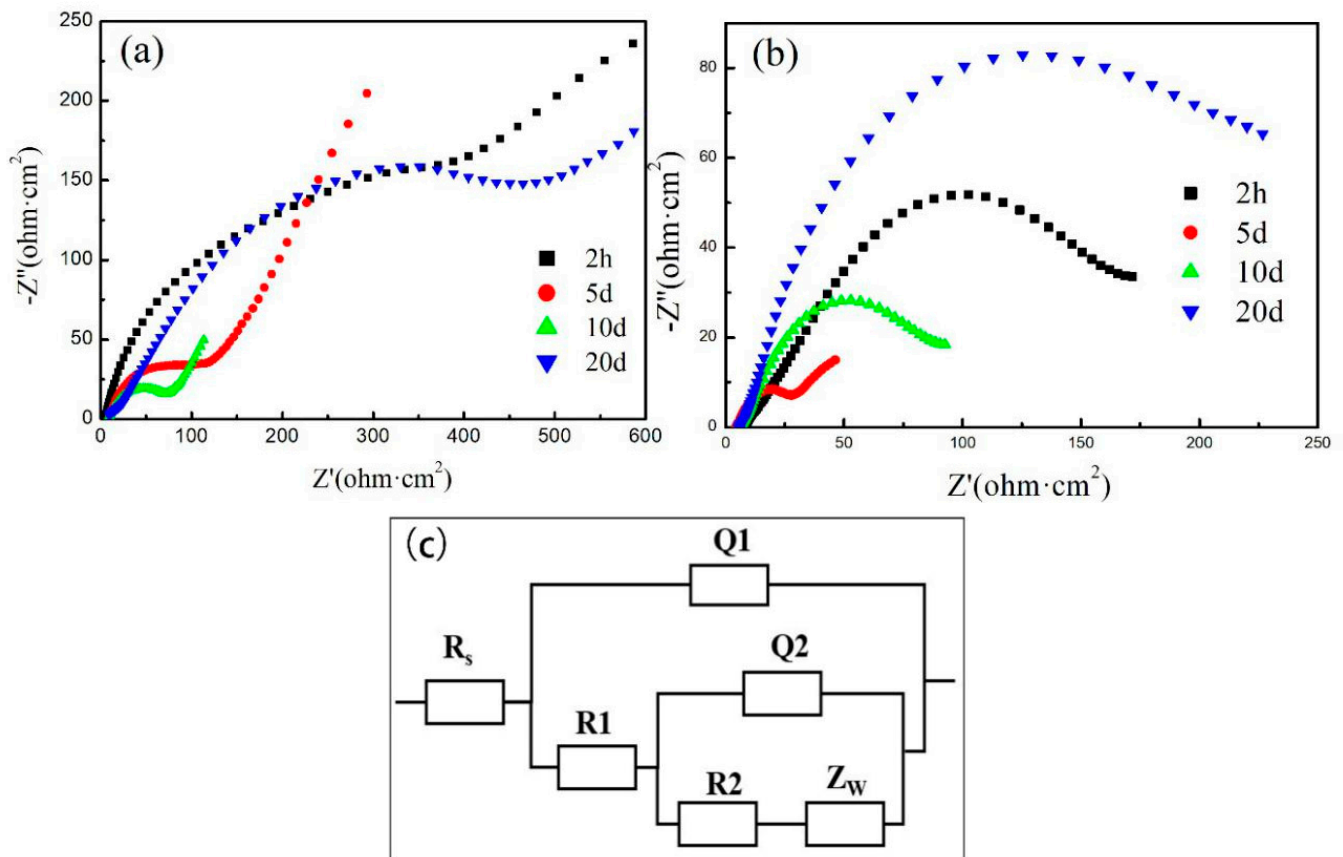


Figure 8. Impedance change for Zn-Al and Zn-0.2 wt.%G/Al coatings during full immersion. (a) Zn-Al. (b) Zn-0.2 wt.%G/Al coating. (c) equivalent circuit model.

The variation in the EIS radius for the coating during mid-term immersion showed that the Zn-x wt.%G/Al coating experienced three phases: the first is the shielding of the coating, the second is the erosion of the coating, which provides cathodic protection, and the third is the barrier of the formed erosion product layer. For the Zn-Al coating, the cathodic protection stage occurred in the first 10 d of immersion. The arc radius increased with immersion time due to the corrosion product layer formed on the Zn-Al coating. Although the service life of the coating can be extended due to the shielding protection of the corrosion product layer, the cathodic protection efficiency is still low, as shown in Table 1 (E_{corr} value of Zn-Al at 20d immersion time is $-1.083 V_{SCE}$, which is higher than that of Zn-x wt.%G/Al coating). For Zn-0.2 wt.%G/Al, the cathodic protection stage occurred in the first 5 d of immersion, and the R_1 value (arc radius value) dramatically decreased. After 5 d immersion, the arc radius value of the EIS curve gradually increased. The increased R_1 value shows that the formed corrosion product layer has a better shielding protection effect. With a further increase in immersion time (after 20 d), the shielding protection effects of the corrosion product layer significantly increased beyond the shielding protection of the Zn-0.2 wt.%G/Al coating at the initial immersion time, as shown by the largest arc radius value of the EIS curve. The excellent protection of the corrosion products on the Zn-0.2 wt.%G/Al coating surface could be the result of the shielding effect of G in the corrosion products. The Zn-0.2 wt.%G/Al coating has a superior cathodic protection efficiency after 20 d immersion (with a lower E_{corr} value of $-1.152 V_{SCE}$), which can be ascribed to the bridge connection with the conductivity of G.

4. Mechanism

According to the results of PPS and EIS, we deduced that the Zn-0.2 wt.%G/Al coating possesses a continuous cathodic protection ability compared with the other three coatings

after 20 d immersion, and the corrosion product on Zn-0.2 wt.%G/Al coating could delay the dissolution of the coating, which could prolong the service life of the coating during the full-immersion process. The special protective properties of the Zn-0.2 wt.%G/Al coating produced during medium-term immersion can be attributed to the equilibrium effect of G. Actually, graphene is a double-edged sword when applied in the corrosion protection of a coating [22]. When G completely coats metal surfaces or is used as an additive in organic or inorganic coatings, G prolongs the propagation path of the corrosive medium through its large specific surface area; thus, the use of G in the coating mainly plays a role in shielding protection [31,32]. However, the conductivity of G is inclined to expedite the metal degradation when G metal matrix composites are used [18]. Due to the potential difference between Zn, Al and G, the reaction process of the Zn-G/Al coating in an aggressive medium involves galvanic reactions. Figure 9 shows the microbattery reaction process of the two coatings soaked in an aggressive NaCl medium.

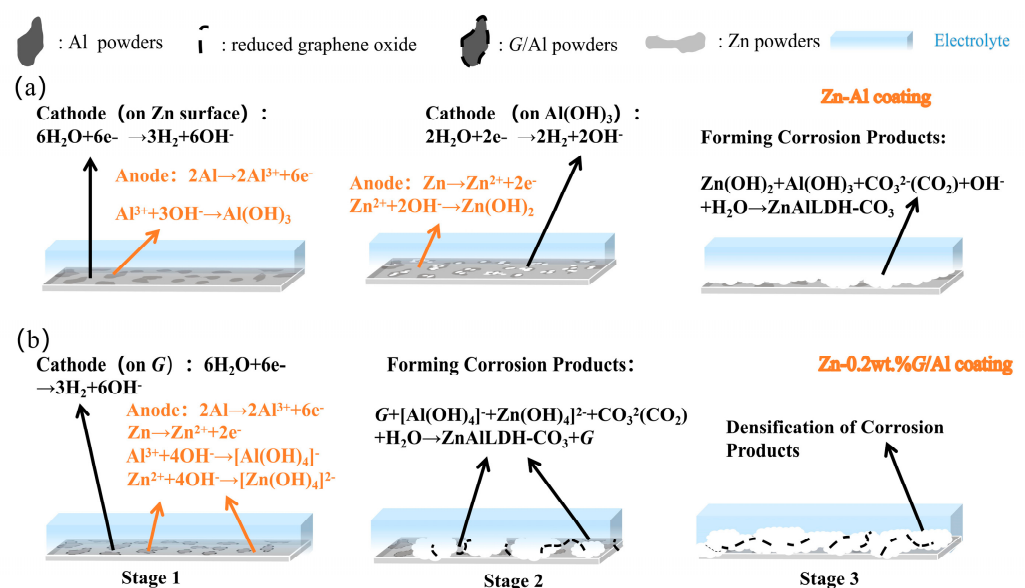


Figure 9. Model for microbattery reaction process of Zn-Al and Zn-0.2 wt.%G/Al coatings during immersion in 3.5 wt.% NaCl solution. (a) Zn-Al coating. (b) Zn-0.2 wt.%G/Al coating.

For the Zn-Al coating (Figure 9a), Al with a low self-corrosion potential is preferentially dissolved and promotes the release of OH^- , by which the 3.5 wt.% NaCl solution gradually becomes alkaline and promotes the dissolution of Zn. The dissolved zinc and aluminum first formed oxides that were easily hydrolyzed. The oxides hydrolyzed to hydroxides $\text{Zn}(\text{OH})_4^{2-}$ and $\text{Al}(\text{OH})_4^-$, which continuously promote the dissolution of the coating. When the hydroxide content in solution is high enough, hydroxides coordinate to form stable bimetallic hydroxides and deposit on the coating surface. In the Zn-G/Al coating (Figure 9b), the addition of conductive G transforms Zn and Al into anode, so that Zn and Al dissolve simultaneously and promote the formation of corrosion products, as demonstrated in Figure 2. During the corrosion product layer formation, the solvent-less G in the Zn-Al coating was exposed by the dissolution of Zn and Al and entered into the corrosion product layer, accompanied by the stacking of corrosion products. According to the XRD results exhibited in Figure 4, corrosion products mainly consist of LDH. LDH is an inorganic compound with an impotent electron conductivity, which would weaken the cathodic protection property of the Zn-Al coating. G in the corrosion product layer acts as both a barrier and means of electron conduction. Firstly, the barrier property of G prolongs the permeation path of the erosion media, which enhanced the shielding ability of the corrosion product film. Secondly, G in the corrosion product layer bridged the coating and the corrosive medium and facilitated electron propagation, which provided the coating with continuous cathodic protection.

Among the four coatings, we deduced that the Zn-0.2 wt.%G/Al coating possesses a continuous cathodic protection ability, and the corrosion product film generated on Zn-0.2 wt.%G/Al coating after immersion in the medium has the best shielding ability. This phenomenon is related to the distribution and concentration of G in the coating. In our previous work, we proved that the deposition effect of Al powders is strongly associated with the G concentration when coated on Al. During cold spraying, properly increasing the difference in hardness between the sprayed particles can enhance the particle deposition efficiency; however, an exorbitant particle hardness will cause particles to violently rebound. G possesses an excellent mechanical strength; metal materials combined with G have a significantly enhanced hardness. In addition, a mechanically bonded heterogeneous interface is formed between G and Zn particles during cold spraying; therefore, with an increase in G concentration on the Al surface, the interface energy between G and Zn will increase and the G/Al in the coating will be distributed more evenly. In the Zn-Al coating, poorly dispersed Al agglomerates are found. When the G-coated Al is applied, the distribution of Al becomes uniform; moreover, G/Al in the Zn-0.2 wt.%G/Al composite coating is significantly decreased and uniformly scattered. When the concentration of G coated on Al is increased to 0.3 wt%, the main component of the coating is Zn, due to the rebound of 0.3 wt.%G/Al. Therefore, among the four coatings, the Zn-0.2 wt.%G/Al coating is equipped with a continuous cathodic protection ability and the corrosion products on the Zn-G/Al coating surface have better shielding properties than the initial Zn-G/Al coating due to the shielding of G, which could delay the dissolution of that coating when dipped in aggressive solution.

5. Conclusions

In this work, the corrosion behavior of a Zn-x wt.%G/Al coating in an aggressive NaCl solution was explored. Results indicated the Zn-0.2 wt.%G/Al coating is equipped with a continuous cathodic protection ability and formed a protective layer of corrosion products on the Zn-G/Al coating surface with better shielding properties than the initial Zn-G/Al coating, which could delay the dissolution of that coating when dipped in aggressive solution.

The special protective properties of the Zn-0.2 wt.%G/Al coating can be attributed to the equilibrium effect of G. Firstly, G in Zn-0.2 wt.%G/Al coating could facilitate the dissolution of the initial coating and, at the same time, the conductivity of G in the corrosion product layer bridged the coating and the corrosive medium and facilitated electron propagation, which provided the coating with continuous cathodic protection. Secondly, the barrier G in the corrosion product layer could prolong the permeation path of the aggressive medium, which enhanced the shielding ability of the corrosion product film.

Author Contributions: Methodology, Q.S.; Resources, D.W. and J.W.; Writing—original draft, Q.S.; Writing—review & editing, H.W.; Supervision, P.Z. and X.J. All authors have read and agreed to the published version of the manuscript.

Funding: This research was funded by Guangdong Social Science and Technology Development Key Project (No. 2021A1515110154), Natural Science Foundation of Anhui Province (No. 2008085ME149), Natural Science Foundation of Anhui Province (No. 2308085QE132, No. 2308065ME171), Anhui University Scientific Research Project (No. 2023AH051660, No. 2022AH040247).

Institutional Review Board Statement: Not applicable.

Informed Consent Statement: Not applicable.

Data Availability Statement: Not applicable.

Conflicts of Interest: The authors declare no conflict of interest.

References

1. Pourhashem, S.; Seif, A.; Saba, F.; Nezhad, E.G.; Ji, X.; Zhou, Z.; Zhai, X.; Mirzaee, M.; Duan, J.; Rashidi, A.; et al. Antifouling nanocomposite polymer coatings for marine applications: A review on experiments, mechanisms, and theoretical studies. *J. Mater. Sci. Technol.* **2022**, *118*, 73–113. [[CrossRef](#)]
2. Ou, Y.; Wang, H.; Hua, Q.; Liao, B.; Ouyang, X. Tribocorrosion behaviors of superhard yet tough Ti-C-N ceramic coatings. *Surf. Coat. Technol.* **2022**, *439*, 128448. [[CrossRef](#)]
3. Xu, M.; Lam, C.C.; Wong, D.; Asselin, E. Evaluation of the cathodic disbondment resistance of pipeline coatings—A review. *Prog. Org. Coat.* **2020**, *146*, 105728. [[CrossRef](#)]
4. Arrighi, C.; Nguyen, T.T.; Paint, Y.; Coelho, C.S.; Coelho, L.B.; Creus, J.; Olivier, M.G. Study of Ce(III) as a potential corrosion inhibitor of Zn-Fe sacrificial coatings electrodeposited on steel. *Corros. Sci.* **2022**, *200*, 110249. [[CrossRef](#)]
5. Luo, Q.; Li, Q.; Zhang, J.Y.; Lu, H.S.; Li, L.; Chou, K.C. Microstructural evolution and oxidation behavior of hot-dip 55 wt.% Al-Zn-Si coated steels. *J. Alloys Compd.* **2015**, *646*, 843–851. [[CrossRef](#)]
6. Malihe, Z.; Hossein, A.; Parvin, G.; Singh, C.N.P.; Sargazi, G. Application of Artificial Neural Networks for Corrosion Behavior of Ni-Zn Electrophosphate Coating on Galvanized Steel and Gene Expression Programming Models. *Front. Mater.* **2022**, *9*, 823155.
7. Wu, P.P.; Song, G.L.; Zhu, Y.X.; Zheng, D.J. Intelligentization of traditional sacrificial anode Zn by Mg-alloying for reinforcing steel. *Corros. Sci.* **2022**, *194*, 109943. [[CrossRef](#)]
8. Shimpei, T.; Izumi, M.; Yu, S.; Takahashi, M.; Matsumoto, M.; Nobuyoshi, H. Micro-electrochemical investigation on the role of Mg in sacrificial corrosion protection of 55mass%Al-Zn-Mg coated steel. *Corros. Sci.* **2017**, *129*, 126–135.
9. Tachiban, K.; Morina, Y.; Mayuzumi, M. Hot dip fine Zn and Zn–Al alloy double coating for corrosion resistance at coastal area. *Corros. Sci.* **2007**, *49*, 149–157. [[CrossRef](#)]
10. Azevedo, M.S.; Allély, C.; Ogle, K.; Volovitch, P. Corrosion mechanisms of Zn (Mg, Al) coated steel: 2. The effect of Mg and Al alloying on the formation and properties of corrosion products in different electrolytes. *Corros. Sci.* **2015**, *90*, 482–490. [[CrossRef](#)]
11. Xue, Q.; Sun, C.Y.; Yu, J.Y.; Huang, L.; Wei, J.; Zhang, J. Microstructure evolution of a Zn-Al coating co-deposited on low carbon steel by pack cementation. *J. Alloys Compd.* **2017**, *699*, 1012–1021. [[CrossRef](#)]
12. Zhu, Z.X.; Xu, B.X.; Chen, Y.X. Effect of Al Content on Electrochemical Corrosion Behavior of Arc Sprayed Zn-Al Coating. *China Surf. Eng.* **2011**, *24*, 58–61.
13. Kim, J.H.; Lee, M.H. A Study on Cavitation Erosion and Corrosion Behavior of Al-, Zn-, Cu-, and Fe-based Coatings Prepared by Arc Spraying. *J. Therm. Spray Technol.* **2010**, *19*, 1224–1230. [[CrossRef](#)]
14. Darabi, A.; Azarmi, F. Investigation on relationship between microstructural characteristics and mechanical properties of wire-arc-sprayed Zn-Al coating. *J. Therm. Spray Technol.* **2020**, *29*, 297–307. [[CrossRef](#)]
15. Huang, G.S.; Lou, X.D.; Wang, H.R.; Li, X.B.; Xing, L.K. Investigation on the Cathodic Protection Effect of Low Pressure Cold Sprayed AlZn Coating in Seawater via Numerical Simulation. *Coatings* **2017**, *7*, 93. [[CrossRef](#)]
16. Liu, W.; Li, M.C.; Luo, Q.; Fan, H.Q.; Zhang, J.Y.; Lu, H.S.; Chou, K.C.; Wang, X.L.; Li, Q. Influence of alloyed magnesium on the microstructure and long-term corrosion behavior of hot-dip Al-Zn-Si coating in NaCl solution. *Corros. Sci.* **2016**, *104*, 217–226. [[CrossRef](#)]
17. Zhu, L.Q.; Xu, B.P.; Zhou, M.X.; Hu, S.J.; Zhang, G.D. Fabrication and characterization of Al-Zn-Cu composite coatings with different Cu contents by cold spraying. *Surf. Eng.* **2020**, *36*, 1090–1096. [[CrossRef](#)]
18. Sun, J.L.; Chen, Y.; Zhai, P.; Zhou, Y.H.; Zhao, J.; Huang, Z.F. Tribological performance of binderless tungsten carbide reinforced by multilayer graphene and SiC whisker. *J. Eur. Ceram. Soc.* **2022**, *42*, 4817–4824. [[CrossRef](#)]
19. Zhang, Y.M.; Sun, J.L.; Xiao, X.Z.; Wang, N.; Meng, G.Z.; Gu, L. Graphene-like two-dimensional nanosheets-based anticorrosive coatings: A review. *J. Mater. Sci. Technol.* **2022**, *129*, 139–162. [[CrossRef](#)]
20. Chen, Y.N.; Wu, L.; Yao, W.H.; Wu, J.H.; Xiang, J.P.; Dai, X.W.; Wu, T.; Yuan, Y.; Wang, J.F.; Jiang, B.; et al. Development of metal-organic framework (MOF) decorated graphene oxide/MgAl-layered double hydroxide coating via microstructural optimization for anti-corrosion micro-arc oxidation coatings of magnesium alloy. *J. Mater. Sci. Technol.* **2022**, *130*, 12–26. [[CrossRef](#)]
21. Wang, X.J.; Zhang, L.Y.; Zhou, X.L.; Wu, W.; Jie, X.H. Corrosion behavior of Al₂O₃-reinforced graphene encapsulated Al composite coating fabricated by low pressure cold spraying. *Surf. Coat. Technol.* **2020**, *386*, 125486. [[CrossRef](#)]
22. Muhammad, R.; Pan, F.S.; Muhammad, A.; Chen, X.H. Corrosion behavior of magnesium-graphene composites in sodium chloride solutions. *J. Magnes. Alloys* **2017**, *5*, 271–276.
23. Ding, R.; Zheng, Y.; Yu, H.B.; Li, W.H.; Wang, X.; Gui, T.J. Study of water permeation dynamics and anti-corrosion mechanism of graphene/zinc coatings. *J. Alloys Compd.* **2018**, *748*, 481–495. [[CrossRef](#)]
24. Wu, H.S.; Zhang, L.Y.; Liu, C.S.; Mai, Y.J.; Zhang, Y.C.; Jie, X.H. Deposition of Zn-G/Al composite coating with excellent cathodic protection on low carbon steel by low-pressure cold spraying. *J. Alloys Compd.* **2020**, *821*, 153483. [[CrossRef](#)]
25. Wu, H.S.; Shen, G.Z.; Li, R.X.; Zhang, L.Y.; Jie, X.H.; Liu, G. Influence of embedded reduced graphene oxide on the corrosion-wear performance of cold sprayed Zn-rGO/Al coating in NaCl solution. *Surf. Coat. Technol.* **2022**, *429*, 127856. [[CrossRef](#)]
26. Chen, M.; Wang, Y.; Song, L.; Gunawan, P.; Zhong, Z.; She, X.; Su, F. Urchin-like ZnO microspheres synthesized by thermal decomposition of hydrozincite as a copper catalyst promoter for the Rochow reaction. *RSC Adv.* **2012**, *2*, 4164–4168. [[CrossRef](#)]
27. Elvins, J.; Spittle, J.A.; Sullivan, J.H.; Worsley, D.A. The effect of magnesium additions on the microstructure and cut edge corrosion resistance of zinc aluminium alloy galvanised steel. *Corros. Sci.* **2008**, *50*, 1650–1658. [[CrossRef](#)]

28. Prosek, T.; Hagström, J.; Persson, D.; Fuertes, N.; Lindberg, F.; Chocholatý, O.; Taxén, C.; Šerák, J.; Thierry, D. Effect of the microstructure of Zn-Al and Zn-Al-Mg model alloys on corrosion stability. *Corros. Sci.* **2016**, *110*, 71–81. [[CrossRef](#)]
29. Oliveira, C.G.; Ferreira, M. Ranking high-quality paint systems using EIS. Part II: Defective coatings. *Corros. Sci.* **2003**, *45*, 139–147. [[CrossRef](#)]
30. Mouanga, M.; Bercot, P. Comparison of corrosion behaviour of zinc in NaCl and in NaOH solutions; Part II: Electrochemical analyses. *Corros. Sci.* **2010**, *52*, 3993–4000. [[CrossRef](#)]
31. Ding, R.; Li, W.; Wang, X.; Gui, T.; Li, B.; Han, P.; Tian, H.; Liu, A.; Wang, X.; Liu, X.; et al. A brief review of corrosion protective films and coatings based on graphene and graphene oxide. *J. Alloys Compd.* **2018**, *764*, 1039–1055. [[CrossRef](#)]
32. Sun, J.; Martinsen, K.H.; Klement, U.; Kovtun, A.; Xia, Z.; Silva, P.F.B.; Hryha, E.; Nyborg, L.; Palermo, V. Controllable Coating Graphene Oxide and Silanes on Cu Particles as Dual Protection for Anticorrosion. *ACS Appl. Mater. Interfaces* **2023**, *15*, 38857–38866. [[CrossRef](#)] [[PubMed](#)]

Disclaimer/Publisher's Note: The statements, opinions and data contained in all publications are solely those of the individual author(s) and contributor(s) and not of MDPI and/or the editor(s). MDPI and/or the editor(s) disclaim responsibility for any injury to people or property resulting from any ideas, methods, instructions or products referred to in the content.